Fbrsl1 is required for heart development in *Xenopus laevis* and de novo variants in FBRSL1 can cause human heart defects

Hanna Berger[1,‡], Sarah Gerstner[1,‡], Marc-Frederik Horstmann[1], Silke Pauli[2] and Annette Borchers[1,*]

[1]Department of Biology, Molecular Embryology, Philipps-University Marburg, Marburg, Germany
[2]Institute of Human Genetics, University Medical Center Göttingen, Heinrich-Düker-Weg 12, 37073 Göttingen, Germany

*Corresponding Author: borchers@uni-marburg.de, ORCID-ID: 0000-0002-2524-5384
‡Hanna Berger and Sarah Gerstner contributed equally to this work.

Abstract

De novo truncating variants in *Fibrosin-like protein 1* (*FBRSL1*), a member of the *AUTS2* gene family, cause a disability syndrome, including organ malformations such as heart defects. Here, we use *Xenopus laevis* to investigate whether Fbrsl1 plays a role in heart development. *Xenopus laevis fbrsl1* is expressed in tissues relevant for heart development and morpholino-mediated knockdown of Fbrsl1 results in severely hypoplastic hearts. Our data suggest that Fbrsl1 is required for the development of the first heart field, which contributes to the ventricle and the atria, but not for the second heart field, which gives rise to the outflow tract. The morphant heart phenotype could be rescued using a human N-terminal FBRSL1 isoform that contains an alternative exon, but lacks the AUTS2 domain. N-terminal isoforms carrying patient variants failed to rescue. Interestingly, a long human FBRSL1 isoform, harboring the AUTS2 domain, did also not rescue the morphant heart defects. Thus, our data suggest that different FBRSL1 isoforms may have distinct functions and that only the short N-terminal isoform, appears to be critical for heart development.

Keywords: congenital malformation syndrome, heart development, Fbrsl1, AUTS2

Introduction

We recently identified truncating variants in the *FBRSL1* gene in three unrelated children showing strikingly similar malformations (Pauli et al., 2021; Ufartes et al., 2020). The patients present with facial dysmorphism, cleft palate, microcephaly, skeletal anomalies and contractures, skin creases, developmental delay and growth retardation. Respiratory problems, hearing impairment and heart defects have also been observed. All variants cluster in the N-terminal region of the FBRSL1 protein encoded by exons 2 and 3 and lead to premature stop codons, whereby the severity of the malformations increases with the distance of the variant from the ATG region. Two severely affected children, carrying either the *FBRSL1* variant c.487C>T or the deletion c.581_603del, were diagnosed at birth, when they showed respiratory and feeding problems in combination with craniofacial anomalies and excessive skin folds at the arms, legs and back (Ufartes et al., 2020). Furthermore, these children also had heart defects, one an atrial septal defect (ASD) in combination with a persistent ductus arteriosus, the other an atrial and ventricular septal defect (VSD) (Ufartes et al., 2020). Thus, FBRSL1 likely plays distinct roles during embryonic development.

The function of FBRSL1 in embryonic development has so far not been well characterized. In zebrafish, *fbrsl1* is expressed in the developing brain, the spinal cord, the cranial ganglia and the somites (Kondrychyn et al., 2017). In *Xenopus laevis*, we have shown that *fbrsl1* is expressed throughout early development (Ufartes et al., 2020). At tailbud stages, *fbrsl1* transcripts are detected in the branchial arches, the cranial nerves and the brain. Furthermore, morpholino-mediated knockdown of Fbrsl1 resulted in craniofacial defects and a reduction in brain size on the injected side. In addition, the migration of cranial and motor neurons was impaired (Ufartes et al., 2020). As patients carrying *FBRSL1* variants also have heart defects, it is likely that Fbrsl1 plays a role in heart development.

Vertebrate heart development is an evolutionarily conserved process that can be well studied using the *Xenopus* system (Duncan and Khokha, 2016; Hempel and Kuhl, 2016; Hoppler and Conlon, 2020; Kaltenbrun et al., 2011; Kostiuk and Khokha, 2021; Warkman and Krieg, 2007). Advantages include the rapid external

development of embryos, established techniques for tissue-specific micromanipulation and the fact that embryos can survive to early tadpole stages without a functional circulatory system (Hempel and Kuhl, 2016; Hoppler and Conlon, 2020). The *Xenopus* three-chambered heart consists of two atria and a single ventricle and represents an intermediate between the two-chambered heart of the fish and the four-chambered heart of birds and mammals (Gessert and Kuhl, 2009). *Xenopus* cardiogenesis begins at gastrulation, when the precardiac mesoderm forms on the dorsal side, adjacent to both sides of the Spemann's organizer (Nascone and Mercola, 1995; Sater and Jacobson, 1989; Sater and Jacobson, 1990). During gastrulation these cells move anterior to the ventral midline, where they fuse to form a crescent-shaped structure that will divide into the first heart field (FHF) and the second heart field (SHF) (Gessert and Kuhl, 2009). The *Xenopus* FHF will give rise to the ventricle and the two atria, while the SHF will form the outflow tract. In contrast to amniotes, outflow tract septation in *Xenopus* relies solely on the second heart field and not the cardiac neural crest cells (Lee and Saint-Jeannet, 2011). Key stages of heart development were defined by comparative analysis of the spatio-temporal expression pattern of cardiac marker genes and morphological features (Gessert and Kuhl, 2009; Kolker et al., 2000; Mohun et al., 2000). These can now serve as reference points for functional analysis. Here, we use the *Xenopus* system to analyze the function of Fbrsl1 in heart development.

Results

Fbrsl1 is expressed in the developing *Xenopus* heart

In order to study the function of Fbrsl1 in *Xenopus* heart development, we first analyzed the *fbrsl1* expression pattern using an antisense probe detecting *Xenopus laevis* full-length *fbrsl1*. Consistent with our previously published temporal *fbrsl1* expression pattern analyzed by RT-PCR (Ufartes et al., 2020), whole-mount in situ hybridization demonstrated *fbrsl1* expression at all stages analyzed, starting from fertilized oocytes to tailbud stages (Fig. 1). Maternal *fbrsl1* expression was detected in the animal pole at stage 2 (Fig. 1A,B), followed by a broad *fbrsl1* expression during gastrulation, with the exception of the blastoporus (Fig. 1C). No staining was observed using the full-length *fbrsl1* sense probe as a control (Fig. 1D). At early

neurula stages, *fbrsl1* expression was detected in the anterior neural plate, while this area was not stained using the *fbrsl1* sense control (Fig. 1E and data not shown). At these stages, the cardiac progenitor cells localize in an area, which encompasses the crescent-shaped *fbrsl1*-expressing cells at the anterior end. For example, *nkx2.5* (Fig. 1F) or *isl1* (Fig. 3H) are expressed in an anterior domain (Gessert and Kuhl, 2009) covering the area of the *fbrsl1*-expressing cells. However, at neurula stages, where cardiac markers show a distinct expression domain ventral to the cement gland (Gessert and Kuhl, 2009), *fbrsl1* expression is not detected in this domain. Nevertheless, there is a general enrichment of *fbrsl1* expression in the anterior region of the embryo, which may argue for a function in early heart development. *Fbrsl1* also continues to be expressed in the closed neural tube, with an enrichment in the future brain area. Furthermore, *fbrsl1* expression is detected in migratory cranial neural crest cells (Fig. 1G-I; Fig. 1J, sense control). At tailbud stages, *fbrsl1* is expressed in the neural tube, the branchial arches, the brain, the otic vesicle and the proctodeum (Fig. 1K,L). Consistent with a potential role in heart development, *fbrsl1* expression is detected in the heart at late tailbud stages (Fig. 1L). Heart expression is also seen at free-swimming tadpole stages, but not detected in the *fbrsl1* sense controls (Fig. 1M,N). Transverse sections confirm that *fbrsl1* is expressed in the ventricle of free-swimming tadpoles (Fig. 1O,P). In addition, free-swimming tadpoles show *fbrsl1* expression in the branchial arches and the brain (Fig.1 M). Taken together, the *fbrsl1* spatial expression pattern is consistent with a potential function in *Xenopus* heart development.

Fbrsl1 loss-of-function causes defects in heart development

To analyze whether Fbrsl1 loss-of-function affects heart morphology we used loss-of-function studies. To this end, two distinct morpholino oligonucleotides were used to knockdown Fbrsl1 in *Xenopus laevis* embryos: first, the previously published *fbrsl1* splice-blocking morpholino (Ufartes et al., 2020), hereafter referred to as *fbrsl1* sp MO, and second, a *fbrsl1* translation blocking morpholino, hereafter referred to as *fbrsl1* tb MO (Fig. 2A). The splice-blocking morpholino (*fbrsl1* sp MO) blocks splicing at the exon 1/intron 1 boundary, leading to the inclusion of intron 1 and the generation of novel in-frame stop codons, resulting in a severe truncation of the protein (Ufartes et al., 2020). The effectiveness of the *fbrsl1* tb MO was verified by western blot analysis (supplementary Fig. S1) showing that it inhibits the translation

of a GFP-labeled *Xenopus laevis* fbrsl1-transcript containing the *fbrsl1* tb MO binding site. The different morpholino oligonucleotides were unilaterally targeted to the cardiac mesoderm and heart morphology was analyzed at tadpole stages. This strategy allows to directly compare the injected and uninjected (control) side in a single embryo, which is of advantage to analyze early stages of heart development, where markers are bilateral symmetrically expressed. The injected embryos were analyzed by in situ hybridization for *mhc*α (alpha-myosin heavy chain), which is expressed in the myocardium, including the ventricle, atria, and outflow tract, as well as the jaw muscles (Garriock et al., 2005). Wild-type embryos had no defects (Fig. 2B left panel, Fig. 2D) and distinct structures of the heart could be distinguished. Similar to wild-type embryos, control MO injected embryos showed only few, minor defects (Fig. 2B, right panel, Fig. 2D). In contrast, *fbrsl1* morphant embryos showed severe defects in heart formation, which ranged from hypoplastic hearts to the complete absence of the heart (Fig. 2C,D). In addition, heart defects were quantified at tadpole stages by fluorescent imaging of embryos immunostained for cardiac muscle troponin T (CT3) or myosin heavy chain (MF20) (images not shown), confirming the data obtained by in situ hybridization for *mhc*α (Fig. 2E).

Next, live-imaging was used to further analyze beating heart morphology in free-swimming tadpole embryos. While wild-type or control morpholino (Co MO) injected embryos showed a normal heart morphology, (Fig. 2F,G), depletion of Fbrsl1 by either the *fbrsl1* sp MO or the *fbrsl1* tb MO resulted in severe hypoplasia of the heart (Fig. 2H,I). Interestingly, we observed that the outflow tracts were the least affected structure in the morphant hearts, while the ventricular defects appeared more severe. To test whether this observation is correct, we used live-imaging of injected and wild-type tadpole embryos and measured the length and the width of the outflow tract as well as the area of the ventricle at the time point of contraction (Fig. 2J). Indeed, the length and width of the outflow tract was not significantly affected (Fig. 2K,L), while the ventricle area decreased in *fbrsl1* morphant embryos (Fig. 2M).

To further asses ventricle morphology in detail, high-resolution fluorescence microscopy of CT3 stained tadpole embryos was used (Fig. 2N-Q). Z-stacks were recorded and the depth of the z-stacks was visualized using a color-code. While

wild-type and control MO injected embryos (Fig. 2N,O) showed a regular oval-shaped ventricle, Fbrsl1 loss-of-function caused severe defects in ventricle formation (Fig. 2P,Q). The ventricle of *fbrsl1* morphant embryos were smaller, irregular shaped and the cardiac tissue appeared severely disorganized (Fig. 2P,Q). Taken together, and in light of the findings that variants in *FBRSL1* in humans cause heart defects (Ufartes et al., 2020), these data support a function of Fbrsl1 in heart development.

Fbrsl1 is not required for cardiac mesoderm induction, but for the formation of the first heart field

To determine at which stages of heart development Fbrsl1 is required, we analyzed cardiac marker expression at different stages of heart development (Fig. 3A). We started our analysis at the tailbud stage to analyze whether fbrsl1 loss of function affects cardiac differentiation, which was again assessed by *mhc*α expression, as a marker for the earliest stages of cardiac differentiation. Consistent with the severe defects seen at tadpole stages, the morphant embryos showed a strong reduction in *mhc*α expression on the injected side compared to the control side, while control embryos looked normal (Fig. 3B,C). Thus, cardiac differentiation appears to be impaired by Fbrsl1 loss-of-function. Furthermore, these data indicate that the development of the first heart field is inhibited, as *mhc*α is expressed at these stages in the first heart field (Gessert and Kuhl, 2009). Next, we analyzed the development of the second heart field by performing *islet* 1 (*isl1)* in situ hybridization, which marks the second heart field (Brade et al., 2007). Here, we did not observe any significant defects (Fig. 3D,E), suggesting that the development of the second heart field is not affected. To determine whether Fbrsl1 is also involved in earlier stages of heart development, we analyzed the expression of *nkx2.5*, a transcription factor that marks the development of the first and second heart field (Brade et al., 2007; Newman and Krieg, 1998). We observed a significant reduction in *nkx2.5*. expression on the injected side (Fig. 3F,G), indicating a role in lineage specification of the first and second heart fields. Finally, we used *isl1* in situ hybridization to assess the development of the precardiac precursors. Interestingly, we did not observe any defects, suggesting that this early step in heart development is not affected by loss of Fbrsl1 function (Fig. 3H,I). These data suggest that Fbrsl1 is required for the

development of the first heart field, which is relevant for the development of the ventricle and the two atria.

The short N-terminal isoform of FBRSL1 is relevant for heart development

To determine whether the observed defects of *fbrsl1* morphants were specific to loss of Fbrsl1 function, we performed rescue experiments. We recently showed that our patients carried variants in a short N-terminal isoform of *FBRSL1*, which lacks the AUTS2 family domain, but includes a predicted DNA translocase domain (Ftsk) (NCBI conserved database, CDD) (Ufartes et al., 2020). The position of the identified variants (p.W111, p.Q163) as well as a 23 base pair deletion are indicated in Fig. 4A. For rescue experiments, morpholino oligonucleotides alone or in combination with the respective FBRSL1 plasmids, were injected into one blastomere at the four-cell stage and heart development was analyzed at tailbud stages by *mhc*α whole mount in situ hybridization. As expected, injection of the *fbrsl1* sp MO significantly reduced *mhcα* expression on the injected side of the embryo, while wild-type or Co MO injected embryos showed the typical *mhcα* expression in the first heart field (Fig. 4B,C). Co-injection of the long human FBRSL1 isoform I1, which contains the AUTS2 domain, but lacks the alternative exon 3 encoded by the short N-terminal isoform I3.1 (Fig.4A), was not able to rescue the *fbrsl1* morphant phenotype. In contrast, co-injection of the short N-terminal isoform 3.1 (I3.1) significantly rescued the *mhcα* patterning defects caused by Fbrsl1 depletion. However, co-injection of the human FBRSL1 isoform 3.1 (3.I1) carrying the respective patient variants I3.1-p.Gln 163*, I3.1-p.WIII* and I3.1-del were not able to rescue the *mhcα* patterning defects (Fig. 4B,C). Thus, these data indicate that the N-terminal isoform, which carries the alternative exon 3, is relevant for heart development and that the patient variants indeed compromise this function.

Discussion

Congenital heart disease (CHD) is the most common congenital malformation, affecting approximately 1% of newborn each year. More than 400 genes have been implicated in the development of CHD, including transcription factors, chromatin remodelers/modifiers, ciliary genes, myofilament and extracellular matrix genes, and

genes involved in various signaling cascades (e.g. RAS-, Notch-, Wnt-signaling) (Williams et al., 2019). We have recently described a congenital malformation syndrome, caused by heterozygous truncating variants in *FBRSL1*. Two of the three patients presented, in addition to other malformations, with a congenital heart defect. One patient has a hemodynamically relevant ASD, while the other was born with ASD and VSD. A highly variable cardiac phenotype, ranging from mild to severe disease, has been described for various malformation syndromes (e.g. CHARGE syndrome) (Meisner and Martin, 2020). However, due to the small number of patients with FBRSL1-associated syndrome, it is not yet possible to statistically evaluate the range of possible associated heart defects. As heart defects have a significant impact on the clinical outcome of these patients, we have focused our scientific studies on this clinical aspect.

We used the *Xenopus* system to shed light into the function of FBRSL1 in heart development and to test if the patient variants are critically affecting function. We find evidence that Fbrsl1 is required for the development of the first heart field that will later give rise to the ventricle and the atria, which is consistent with the ASD and VSD observed in the patients carrying *FBRSL1* variants. Consistently, *fbrsl1* morphants, showed malformations as well as a reduction in the size of the ventricle at tadpole stages. Interestingly, we did not observe any defects in the formation of the *Xenopus* second heart field, nor did we see significant defects in the formation of the outflow tract. In contrast to amniotes, *Xenopus* cardiac neural crest cells do not appear to migrate into the cardiac cushion and contribute to the septum of the outflow tract (Lee and Saint-Jeannet, 2011). Therefore, we cannot rule out that defects in neural crest migration may also contribute to the clinical phenotype. A role for Fbrsl1 in neural crest development seems likely, because *fbrsl1* morphant embryos show severe craniofacial defects (Ufartes et al., 2020). However, future research is needed to elucidate this role and its implications for heart development.

To date, it is unclear whether the *FBRSL1* variants in patients exert their effect through a loss-of-function or a dominant-negative effect. For our *Xenopus* studies, we used morpholino oligonucleotide injections to knock down Fbrsl1 protein expression. Since we used different embryonic batches, which are also genetically variable, the effectiveness of this strategy will vary from embryo to embryo. This may

explain why some of the embryos showed a complete loss of heart structures, while the defects were less severe in others. This is also supported by the finding that embryos, which lacked heart structures also showed severe defects in craniofacial development. In addition, the severity of defects seems also to increase over time. While the induction of the cardiogenic mesoderm is not affected by a Fbrsl1 knockdown, the severity of defects increased from early to later tailbud stages, suggesting that Fbrsl1 plays a role during subsequent stages of heart development.

To test which isoforms of FBRSL1 are required and whether the patient variants are critically affecting function, we performed rescue experiments. In contrast to AUTS2 syndrome, where the C-terminus containing the AUTS2 domain is mostly relevant (Beunders et al., 2013) the situation is different for the FBRSL1-associated syndrome. Here, only the short human N-terminal FBRSL1 isoform containing an alternative exon 3, which includes a stop codon and thus results in a short protein consisting of only three exons, was able to rescue the developmental heart defects of *fbrsl1* morphant *Xenopus* embryos. This was not possible using the long human FBRSL1 isoform harboring the AUTS2 domain, but lacking exon 3. These findings are also consistent with our previous data showing that the human N-terminal isoform of FBRSL1 – but not the long isoform – rescued *Xenopus* morphant craniofacial defects, indicating that this isoform is relevant for embryonic development. Currently, we do not know if only the N-terminal isoform of FBRSL1 is relevant for embryonic development or if this only holds true for heart and craniofacial development. Especially, considering the importance of AUTS2 for neural development and autism related syndromes (Biel et al., 2022; Pang et al., 2021), the FBRSL1 long isoform, containing an AUTS2 domain potentially also plays a role in neural development, which we know is also affected in *fbrsl1* morphants (Ufartes et al., 2020).

The cellular function of the *FBRSL1* gene and its role in pathogenesis are largely unknown. However, as FBRSL1 and AUTS2 are paralogs, they likely share common conserved functions, which may contribute to the overlapping phenotypes observed in the respective syndromes. FBRSL1 and AUTS2 form – together with Fibrosin (FBRS) – the AUTS2 tripartite gene family (Singh et al., 2015). The members of this protein family share conserved domains, but also have unique regions that likely

contribute to their distinct functions (Sellers et al., 2020). In neurons, a dual function of AUTS2, has been described (Hori and Hoshino, 2017). In the nucleus, it regulates gene transcription as a component of the Polycomb repressive complex (PRC). In addition, it also affects cytoskeletal dynamics by regulating small GTPases of the Rho family (Gao et al., 2014; Hori et al., 2014). For example, AUTS2 activates Rac1 to induce lamellipodia, while it suppresses filopodia formation by downregulating Cdc42 (Hori et al., 2014). Nuclear and cytoplasmic AUTS2 functions are controlled by different domains of the AUTS2 protein: the cytoplasmic function resides in the N-terminal region of the AUTS2 protein, whereas the interaction with the PRC complex is mediated by the C-terminal region (Bedogni et al., 2010; Hori et al., 2014; Oksenberg and Ahituv, 2013; Sellers et al., 2020). Both AUTS2 and FBRSL1 are components of the PRC1.3 and PRC1.5 complexes (Chittock et al., 2017; Gao et al., 2014). The multiprotein PRC complexes act as epigenetic regulators during embryonic development and function as transcriptional repressors. PRC complexes have also been described as transcriptional regulators in heart development (Akerberg and Pu, 2020). Using the *Xenopus* model system, we observed a significant reduction in *nkx2.5* expression in *fbrsl1* morphants. *NKX2.5* is a cardiac transcription factor and heterozygous pathogenic variants lead to congenital heart defects in humans, such as ASD and VSD (Schott et al., 1998). Further studies are required to analyze whether the observed reduction in *nkx2.5* expression is due to a transcriptional misregulation involving the PRC complex or other pathways such as Rac1 or Cdc42 signaling. Interestingly in humans, pathogenic variants in both *RAC1* and *CDC42* have been associated with malformation syndromes, including congenital heart defects. Pathogenic variants in *RAC1* cause the autosomal dominant inherited intellectual developmental disorder type 48 (OMIM # 617751), while heterozygous pathogenic variants in *CDC42* can cause Takenouchi-Kosaki syndrome (OMIM # 616737). Patients with atrial and/or ventricular septal defects have been described in both syndromes (Martinelli et al., 2018; Reijnders et al., 2017; Szczawinska-Poplonyk et al., 2023). Furthermore, Rac1 deficiency in murine neonatal cardiomyocytes leads to defects in lamellipodia formation, cell elongation and polarity, as well as in increased apoptosis and reduced expression of the cardiac transcription factors Gata4, Tbx5, Nkx2.5, and Hand2 (Leung et al., 2014). Thus, although our data show that Fbrsl1 is required for heart development and *FBRSL1*

variants negatively affect this process, future research is required to address the genetics and cellular mechanism by which the variants exert their pathogenic role.

Methods

Xenopus microinjection

All procedures involving *Xenopus* embryos were performed according to the German animal use and care law (Tierschutzgesetz) and approved by the German state administration Hesse (Regierungspräsidium Giessen, V 7/2022). *Xenopus* laevis embryos were obtained and cultured following standard protocols and staged according to the normal table of Nieuwkoop and Faber (Nieuwkoop and Faber, 1956). For microinjection capped sense RNA was synthetized using the mMessage mMachine™ SP6 Transcription Kit (Invitrogen™). The following plasmids were used for *in vitro* transcription: lacZ (Smith and Harland, 1991), mGFP (Moriyoshi et al., 1996) and *X. laevis* GFP-tagged Fbrsl1 isoform A (Fbrsl1_A-eGFP). The *Xenopus laevis fbrsl1* isoform A (2028 bp) is identical to full-length Fbrsl1, but lacks exon 2,3 and most of exon 19. For cloning of Fbrsl1_A-eGFP, *fbrsl1_A* was amplified by PCR from *Xenopus laevis* cDNA using the primer 5'-ATGGATATTAAAACCAAACAACCAAGCAGG-3' and 5'-TATCGTGCCTCCACTTCCTTAGGG-3'. The PCR product was cloned into the pCR™-Blunt II-TOPO™ vector (Zero Blunt™ TOPO™ PCR cloning kit, Thermo Fisher Scientific) and subsequently subcloned into the pCS2+-eGFP vector using the EcoRI and XhoI restriction sites. The following morpholino oligonucleotides (MO) (Gene Tools, LLC) were used for microinjections: Standard control morpholino (Co MO: 5′-CCT CTT ACC TCA GTT ACA ATT TAT A-3′), *fbrsl1* sp MO (Ufartes et al., 2020) and *fbrsl1* tb MO (*fbrsl1* tb: 5'-GGTTGTTTGGTTTTAATATCCATCT-3'). Both, *fbrsl1* sp MO and *fbrsl1* tb MO, target *fbrsl1.L* and show 1 mismatch (*fbrsl1* sp MO) or 4 mismatches (*fbrsl1* tb MO) to *fbrsl1.S* (supplementary Fig. 3). For rescue experiments, plasmids encoding isoform 1, isoform 3.1 and the variant isoform 3.1-p.Gln163 (Ufartes et al., 2020) were co-injected with the *fbrsl1* sp MO. In addition, the non-sense variant, c.332 G > A (p.Trp111*) was introduced by site-directed mutagenesis of variant 3.1 using the QuikChange II XL Site-Directed Mutagenesis Kit (Agilent) according to the manufacturer's protocol and verified by Sanger

sequencing. The construct containing the deletion c.581_603del was generated using patient cDNA. The resulting plasmids were also used for rescue experiments.

Whole-mount immunofluorescence staining of *Xenopus* embryos

Xenopus laevis embryos were injected with Co MO, *fbrsl1* sp MO or *fbrsl1* tb MO in one dorsal blastomere at the four-cell stage, combined with *mGFP* RNA (CT3) or *lacZ* RNA (MF20) as lineage tracer. The embryos were incubated until stage 44, then they were fixed with Dent's fixative (20% DMSO, 80% methanol, for CT3) or MEMFA (3.7% formaldehyde, 0.1 M MOPS, 2 mM EGTA, 2 mM $MgSO_4$, for MF20) and processed for whole mount immunofluorescence staining as previously described (Ufartes et al., 2020). The *Xenopus* heart was visualized by staining against cardiac muscle troponin T (DSHB, CT3 antibody, dilution 1:30) or myosin heavy chain, sarcomere (MHC) (DSHB, MF20 antibody, dilution 1:100). Alexa Fluor® 594 Goat anti-Mouse (Invitrogen™, A-11005, dilution 1:400) was used as secondary antibody.

Whole-mount-in situ hybridization

For the analysis of cardiac marker expression, embryos were injected with either Co MO or *fbrsl1* sp MO at the indicated concentrations together with *lacZ* RNA as lineage tracer in one dorsal blastomere at the four-cell stage. Embryos were fixed using MEMFA (3.7% formaldehyde, 0.1 M MOPS, 2 mM EGTA, 2 mM $MgSO_4$) and β-galactosidase staining and in situ hybridization were performed according to standard protocols (Harland, 1991; Smith and Harland, 1991). The *Xenopus laevis* full-length *fbrsl1* (3609 bp) was amplified by PCR from *Xenopus laevis* cDNA using the primer 5'-ATGGATATTAAAACCAAACAACCAAGCAGG-3' and 5'-TATCGTGCCTCCACTTCCTTAGGG-3'. The PCR product was cloned into the pCR™-Blunt II-TOPO™ vector (Zero Blunt™ TOPO™ PCR cloning kit, Thermo Fisher Scientific), from which sense and antisense RNA probes were synthetized. The *fbrsl1* expression pattern, including sense controls of all documented stages, was analyzed using wild-type embryos. Histological sections of stained embryos were prepared as previously described (Breuer et al., 2020). The following cardiac marker probes were used for functional analysis: *nkx2.5* (Tonissen et al., 1994), *mhcα* (Gessert et al., 2008) and *isl1* (Kelly and Melton, 2000).

Live-imaging of beating hearts

For phenotypic analysis, *Xenopus laevis* embryos were injected in one dorsal blastomere at the four-cell stage with 7.5 ng of the respective morpholino oligonucleotides in combination with 50 pg *mGFP*. For live-imaging of the beating hearts, embryos at stage 44 were anaesthetized in 0.1x MBS (modified Barth's saline) containing 0.01% benzocaine and movies of the beating hearts were recorded. The heart size, the length and width of the OFT and the ventricular area at the time point of contraction were measured using ImageJ.

Imaging and statistical analysis

Phenotypical documentation was performed using a Nikon stereo microscope (SMZ18) with a DS-Fi3 Nikon camera and NIS-Elements imaging software. For immunofluorescence imaging Stellaris 8 Falcon (Leica Microsystems) with LAS X software was used. The investigators were blinded to the group allocation when they assessed the experimental outcome. Statistical analysis was conducted using the one-way ANOVA test with GraphPad PRISM Software (Graphpad Software, Inc.) with the indicated *p* values: *$p \leq 0.05$, **$p \leq 0.01$, ***$p \leq 0.001$, ****$p \leq 0.0001$.

Western blotting

One-cell stage embryos were injected with 10 ng of each morpholino and 100 pg *fbrsl1_A-eGFP* RNA. Ten embryos (stage 20) per condition were lysed in NP-40 lysis buffer (50 mM Tris pH 7.5, 150 mM NaCl, 0.5% (v/v) NP-40 containing 1× Complete Protease Inhibitor (Roche)). The protein extracts were separated by 12 % SDS-PAGE, transferred to a nitrocellulose membrane (AmershamProtran) by electroblotting and blocked in Intercept® (TBS) Blocking Buffer (LI-COR) or TBS buffer (50 mM Tris-HCl pH 7.5, 150 mM NaCl) containing 5 % nonfat dried milk. The following antibodies were used for detection of proteins: anti-GFP (Abcam, ab290, 1:1000) and anti-actin (Merck Millipore, MAB1501, 1:2000) antibodies. Tween-20 was added to the antibody solution at a final concentration of 0.2 %. IRDye®-conjugated secondary antibodies (LI-COR) were used: IRDye® 800CW Donkey anti-Rabbit IgG Secondary Antibody (LI-COR, P/N: 926-32213, 1:7500) and IRDye® 680RD Donkey anti-Mouse IgG Secondary Antibody (LI-COR, P/N 926-68072, 1:7500). Proteins were detected using the Odyssey® Fc Imaging System (LI-COR Bioscience).

Acknowledgements

We thank Roser Ufartes for cloning of the variant constructs for the rescue experiments and Susanne Önel for help with the immunostaining and imaging of the *Xenopus* heart. We also want to thank our former Bachelor students, Marius Luzius, Rebekka Gerloff and Jacob Berger for assisting in this study.

Competing interest

The authors have no relevant financial or non-financial interests to disclose.

Funding

This work was supported by grants of the Deutsche Forschungsgemeinschaft (DFG, German Research Foundation) to A.B. (BO 1978/7-3) and S.P. (PA 2030/5-3).

References

Akerberg, B. N. and Pu, W. T. (2020). Genetic and Epigenetic Control of Heart Development. *Cold Spring Harbor perspectives in biology* **12**.

Bedogni, F., Hodge, R. D., Nelson, B. R., Frederick, E. A., Shiba, N., Daza, R. A. and Hevner, R. F. (2010). Autism susceptibility candidate 2 (Auts2) encodes a nuclear protein expressed in developing brain regions implicated in autism neuropathology. *Gene Expr Patterns* **10**, 9-15.

Beunders, G., Voorhoeve, E., Golzio, C., Pardo, L. M., Rosenfeld, J. A., Talkowski, M. E., Simonic, I., Lionel, A. C., Vergult, S., Pyatt, R. E. et al. (2013). Exonic deletions in AUTS2 cause a syndromic form of intellectual disability and suggest a critical role for the C terminus. *Am J Hum Genet* **92**, 210-20.

Biel, A., Castanza, A. S., Rutherford, R., Fair, S. R., Chifamba, L., Wester, J. C., Hester, M. E. and Hevner, R. F. (2022). AUTS2 Syndrome: Molecular Mechanisms and Model Systems. *Frontiers in molecular neuroscience* **15**, 858582.

Brade, T., Gessert, S., Kuhl, M. and Pandur, P. (2007). The amphibian second heart field: Xenopus islet-1 is required for cardiovascular development. *Developmental Biology* **311**, 297-310.

Breuer, M., Berger, H. and Borchers, A. (2020). Caveolin 1 is required for axonal outgrowth of motor neurons and affects Xenopus neuromuscular development. *Sci Rep* **10**, 16446.

Chittock, E. C., Latwiel, S., Miller, T. C. and Muller, C. W. (2017). Molecular architecture of polycomb repressive complexes. *Biochem Soc Trans* **45**, 193-205.

Duncan, A. R. and Khokha, M. K. (2016). Xenopus as a model organism for birth defects-Congenital heart disease and heterotaxy. *Seminars in Cell & Developmental Biology* **51**, 73-9.

Gao, Z., Lee, P., Stafford, J. M., von Schimmelmann, M., Schaefer, A. and Reinberg, D. (2014). An AUTS2-Polycomb complex activates gene expression in the CNS. *Nature* **516**, 349-54.

Garriock, R. J., Meadows, S. M. and Krieg, P. A. (2005). Developmental expression and comparative genomic analysis of Xenopus cardiac myosin heavy chain genes. *Developmental dynamics : an official publication of the American Association of Anatomists* **233**, 1287-93.

Gessert, S. and Kuhl, M. (2009). Comparative gene expression analysis and fate mapping studies suggest an early segregation of cardiogenic lineages in Xenopus laevis. *Developmental Biology* **334**, 395-408.

Gessert, S., Maurus, D., Brade, T., Walther, P., Pandur, P. and Kuhl, M. (2008). DM-GRASP/ALCAM/CD166 is required for cardiac morphogenesis and maintenance of cardiac identity in first heart field derived cells. *Developmental Biology* **321**, 150-61.

Harland, R. M. (1991). In situ hybridization: an improved whole-mount method for Xenopus embryos. *Methods Cell Biol* **36**, 685-95.

Hempel, A. and Kuhl, M. (2016). A Matter of the Heart: The African Clawed Frog Xenopus as a Model for Studying Vertebrate Cardiogenesis and Congenital Heart Defects. *Journal of cardiovascular development and disease* **3**.

Hoppler, S. and Conlon, F. L. (2020). Xenopus: Experimental Access to Cardiovascular Development, Regeneration Discovery, and Cardiovascular Heart-Defect Modeling. *Cold Spring Harbor perspectives in biology* **12**.

Hori, K. and Hoshino, M. (2017). Neuronal Migration and AUTS2 Syndrome. *Brain Sci* **7**.

Hori, K., Nagai, T., Shan, W., Sakamoto, A., Taya, S., Hashimoto, R., Hayashi, T., Abe, M., Yamazaki, M., Nakao, K. et al. (2014). Cytoskeletal regulation by AUTS2 in neuronal migration and neuritogenesis. *Cell reports* **9**, 2166-79.

Kaltenbrun, E., Tandon, P., Amin, N. M., Waldron, L., Showell, C. and Conlon, F. L. (2011). Xenopus: An emerging model for studying congenital heart disease. *Birth defects research. Part A, Clinical and molecular teratology* **91**, 495-510.

Kelly, O. G. and Melton, D. A. (2000). Development of the pancreas in Xenopus laevis. *Developmental dynamics : an official publication of the American Association of Anatomists* **218**, 615-27.

Kolker, S. J., Tajchman, U. and Weeks, D. L. (2000). Confocal imaging of early heart development in Xenopus laevis. *Developmental Biology* **218**, 64-73.

Kondrychyn, I., Robra, L. and Thirumalai, V. (2017). Transcriptional Complexity and Distinct Expression Patterns of auts2 Paralogs in Danio rerio. *G3 (Bethesda)* **7**, 2577-2593.

Kostiuk, V. and Khokha, M. K. (2021). Xenopus as a platform for discovery of genes relevant to human disease. *Current topics in developmental biology* **145**, 277-312.

Lee, Y. H. and Saint-Jeannet, J. P. (2011). Cardiac neural crest is dispensable for outflow tract septation in Xenopus. *Development* **138**, 2025-34.

Leung, C., Lu, X., Liu, M. and Feng, Q. (2014). Rac1 signaling is critical to cardiomyocyte polarity and embryonic heart development. *J Am Heart Assoc* **3**, e001271.

Martinelli, S., Krumbach, O. H. F., Pantaleoni, F., Coppola, S., Amin, E., Pannone, L., Nouri, K., Farina, L., Dvorsky, R., Lepri, F. et al. (2018). Functional Dysregulation of CDC42 Causes Diverse Developmental Phenotypes. *Am J Hum Genet* **102**, 309-320.

Meisner, J. K. and Martin, D. M. (2020). Congenital heart defects in CHARGE: The molecular role of CHD7 and effects on cardiac phenotype and clinical outcomes. *American journal of medical genetics. Part C, Seminars in medical genetics* **184**, 81-89.

Mohun, T. J., Leong, L. M., Weninger, W. J. and Sparrow, D. B. (2000). The morphology of heart development in Xenopus laevis. *Developmental Biology* **218**, 74-88.

Moriyoshi, K., Richards, L. J., Akazawa, C., O'Leary, D. D. and Nakanishi, S. (1996). Labeling neural cells using adenoviral gene transfer of membrane-targeted GFP. *Neuron* **16**, 255-60.

Nascone, N. and Mercola, M. (1995). An inductive role for the endoderm in Xenopus cardiogenesis. *Development* **121**, 515-23.

Newman, C. S. and Krieg, P. A. (1998). tinman-related genes expressed during heart development in Xenopus. *Developmental Genetics* **22**, 230-8.

Oksenberg, N. and Ahituv, N. (2013). The role of AUTS2 in neurodevelopment and human evolution. *Trends Genet* **29**, 600-8.

Pang, W., Yi, X., Li, L., Liu, L., Xiang, W. and Xiao, L. (2021). Untangle the Multi-Facet Functions of Auts2 as an Entry Point to Understand Neurodevelopmental Disorders. *Front Psychiatry* **12**, 580433.

Pauli, S., Berger, H., Ufartes, R. and Borchers, A. (2021). Comparing a Novel Malformation Syndrome Caused by Pathogenic Variants in FBRSL1 to AUTS2 Syndrome. *Front Cell Dev Biol* **9**, 779009.

Reijnders, M. R. F., Ansor, N. M., Kousi, M., Yue, W. W., Tan, P. L., Clarkson, K., Clayton-Smith, J., Corning, K., Jones, J. R., Lam, W. W. K. et al. (2017). RAC1 Missense Mutations in Developmental Disorders with Diverse Phenotypes. *Am J Hum Genet* **101**, 466-477.

Sater, A. K. and Jacobson, A. G. (1989). The specification of heart mesoderm occurs during gastrulation in Xenopus laevis. *Development* **105**, 821-30.

Sater, A. K. and Jacobson, A. G. (1990). The role of the dorsal lip in the induction of heart mesoderm in Xenopus laevis. *Development* **108**, 461-70.

Schott, J. J., Benson, D. W., Basson, C. T., Pease, W., Silberbach, G. M., Moak, J. P., Maron, B. J., Seidman, C. E. and Seidman, J. G. (1998). Congenital heart disease caused by mutations in the transcription factor NKX2-5. *Science* **281**, 108-11.

Sellers, R. A., Robertson, D. L. and Tassabehji, M. (2020). Ancestry of the AUTS2 family-A novel group of polycomb-complex proteins involved in human neurological disease. *Plos One* **15**, e0232101.

Singh, P. P., Arora, J. and Isambert, H. (2015). Identification of Ohnolog Genes Originating from Whole Genome Duplication in Early Vertebrates, Based on Synteny Comparison across Multiple Genomes. *PLoS Comput Biol* **11**, e1004394.

Smith, W. C. and Harland, R. M. (1991). Injected Xwnt-8 RNA acts early in Xenopus embryos to promote formation of a vegetal dorsalizing center. *Cell* **67**, 753-65.

Szczawinska-Poplonyk, A., Poplonyk, N., Badura-Stronka, M., Juengling, J., Huhn, K., Biskup, S., Bancerz, B. and Walkowiak, J. (2023). The clinical phenotype with gastrostomy and abdominal wall infection in a pediatric patient with Takenouchi-Kosaki

syndrome due to a heterozygous c.191A > G (p.Tyr64Cys) variant in CDC42: a case report. *Front Genet* **14**, 1108852.

Tonissen, K. F., Drysdale, T. A., Lints, T. J., Harvey, R. P. and Krieg, P. A. (1994). XNkx-2.5, a Xenopus gene related to Nkx-2.5 and tinman: evidence for a conserved role in cardiac development. *Developmental Biology* **162**, 325-8.

Ufartes, R., Berger, H., Till, K., Salinas, G., Sturm, M., Altmuller, J., Nurnberg, P., Thiele, H., Funke, R., Apeshiotis, N. et al. (2020). De novo mutations in FBRSL1 cause a novel recognizable malformation and intellectual disability syndrome. *Human genetics*.

Warkman, A. S. and Krieg, P. A. (2007). Xenopus as a model system for vertebrate heart development. *Seminars in Cell & Developmental Biology* **18**, 46-53.

Williams, K., Carson, J. and Lo, C. (2019). Genetics of Congenital Heart Disease. *Biomolecules* **9**.

Zahn, N., James-Zorn, C., Ponferrada, V. G., Adams, D. S., Grzymkowski, J., Buchholz, D. R., Nascone-Yoder, N. M., Horb, M., Moody, S. A., Vize, P. D. et al. (2022). Normal Table of Xenopus development: a new graphical resource. *Development* **149**.

Figures

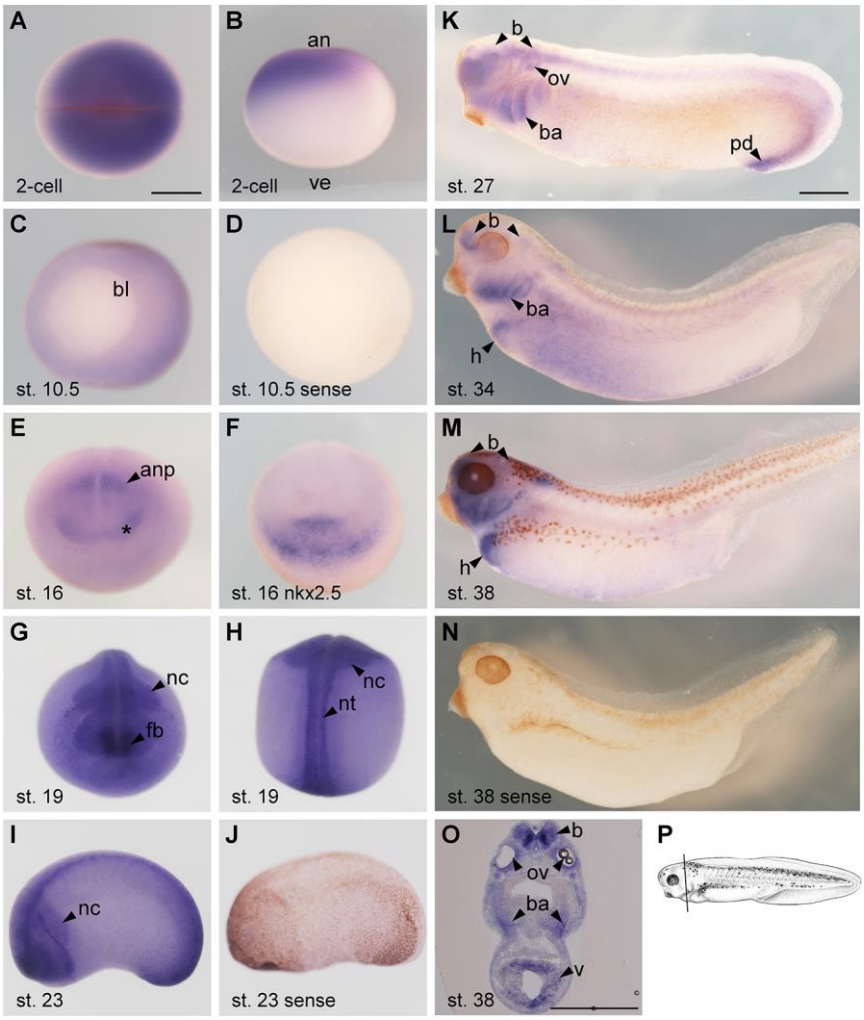

Fig. 1. *Xenopus fbrsl1* spatial expression pattern analyzed by whole mount in situ hybridization. Scale bars = 500 µm. **A,B** Embryo at the two-cell stage, animal view (A), lateral view (B). **C** Embryo at the blastula stage. **D** Embryo at blastula stage, hybridized with the *fbrsl1* sense probe. **E** Embryo at the neurula stage, anterior view, *marks the crescent-shaped expression domain. **F** Embryo at the neurula stage, stained with a *nkx2.5* antisense probe, anterior view. **G,H** Embryo at stage 19, anterior view (G) dorsal view (H). **I** Embryo at stage 23 lateral view. **J** Embryo at stage 23, hybridized with the *fbrsl1* sense probe. **K** Embryo at stage 27, lateral view. **L** Embryo at stage 34, lateral view. **M** Embryo at stage 38, lateral view**. N** Embryo at stage 38, lateral view, hybridized with the *fbrsl1* sense probe. **O** Transversal sections of an embryo at stage 38. **P** Scheme indicating the section

plane of the stage 38 embryo (Zahn et al., 2022) shown in (O). Abbreviations: (an) animal, (anp) anterior neural plate, (b) brain, (ba) branchial arches, (bl) blastoporus, (fb) forebrain, (h) heart, (nc) neural crest, (nt) neural tube, (ov) otic vesicle, (pd) proctodeum, (v) ventricle, (ve) vegetal.

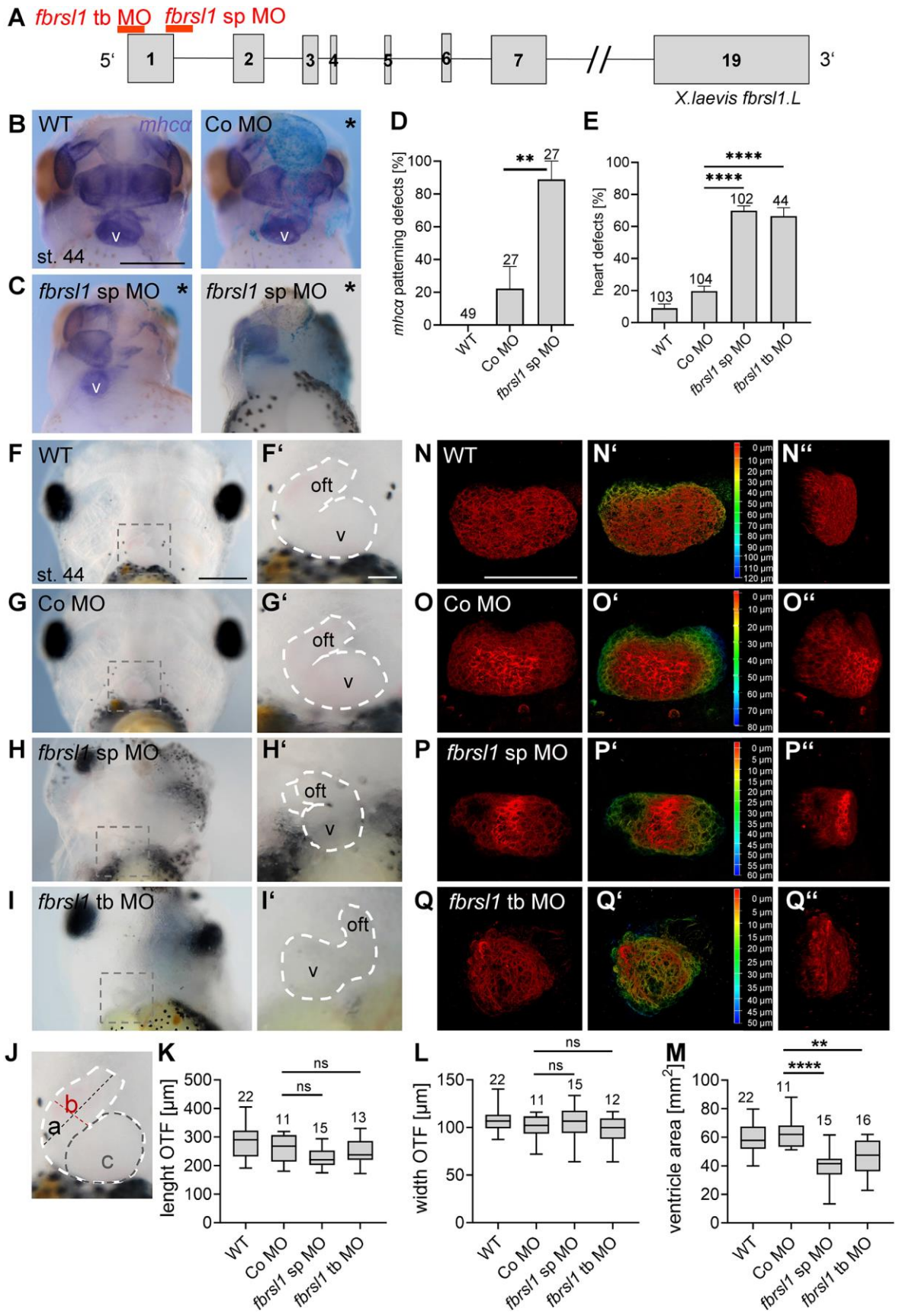

Fig. 2. Fbrsl1 loss-of-function leads to cardiac defects in *Xenopus* embryos. A Scheme showing morpholino binding sites at the 5' region of *Xenopus laevis fbrsl1* (full-length *X. laevis fbrsl1* consists of 19 exons). The *fbrsl1* tb MO targets the translational start site, while the *fbrsl1* sp MO targets the exon1/intron1 boundary (Ufartes et al., 2020). **B,C** Embryos were injected with either 10 ng Co MO or 7.5 ng *fbrsl1* sp MO together with 100 pg *lacZ* RNA as lineage tracer in one dorsal blastomere at the four-cell stage. *Mhcα* in situ hybridization marks the heart and facial muscles in wild-type and morpholino injected embryos. **B** Wild-type and Co MO injected embryos. **C** Embryos injected with *fbrsl1* sp MO. Scale bar = 500 µm. **D** Graph summarizing *mhcα* heart patterning defects of three independent experiments, s.e.m. and number of embryos are indicated, **p= 0.0041 (one-way ANOVA). **E** Embryos were injected with 7.5 ng morpholino oligonucleotides in one dorsal blastomere at the four-cell stage, combined with 50 pg *mGFP* RNA (CT3) or 100 pg *lacZ* RNA (MF20) as lineage tracer. Graph summarizing heart defects of CT3- or MF20-immunostained embryos from at least three independent experiments. Numbers of embryos analyzed (n) and s.e.m. are indicated, ***$p < 0.001$ (one-way ANOVA). **F-I** Four-cell stage embryos were injected in one dorsal blastomere with 7.5 ng of the respective morpholino oligonucleotides in combination with 50 pg *mGFP* RNA as lineage tracers. Heart morphology was analyzed at stage 44, embryos are shown from the ventral side. **F'-I'** Higher magnification of the area marked by squares in F-I. Scale bar represents 500 µm (F-I) or 100 µm (F'-I'). **F, F'** Wild-type and **G,G'** Co MO injected embryos show normal heart morphology. Ventricle (v) and outflow tract (oft) are marked by dashed white lines. **H, H',I, I'** Injection of either the *fbrsl1* sp MO or the *fbrsl1* tb MO leads to defects in heart morphology. **N-Q** Z-stack images of *Xenopus* hearts immunostained for cardiac muscle troponin (CT3). Scale bar = 500 µm**.** **N,O** Oval shape of the heart ventricle in wild-type or Co MO injected embryos. **P,Q** Heart shape and morphology are disturbed after injection of *fbrsl1* sp MO or the *fbrsl1* tb MO. **N'-Q'** Depth color coding profile indicates the extension of the heart ventricles from 0 µm (red) to 50-120 µm (blue), note the different endpoints in N'-Q'. **N''-Q''** XZ-view of heart ventricles. **J-M** Embryos from the experiments shown in **F-I** were used to measure the length of the OTF (a), the width of the OFT (b) and the ventricular area (c) as indicated in **J**. **K-M** Box and whiskers plots summarize the length (**K**) and the width (**L**) of the OFT as well as the ventricular area (**M**). Number of measured hearts, median and whiskers from minimum to maximum are indicated. ns = not significant, **$p < 0.01$, ****$p < 0.0001$ (one-way ANOVA).

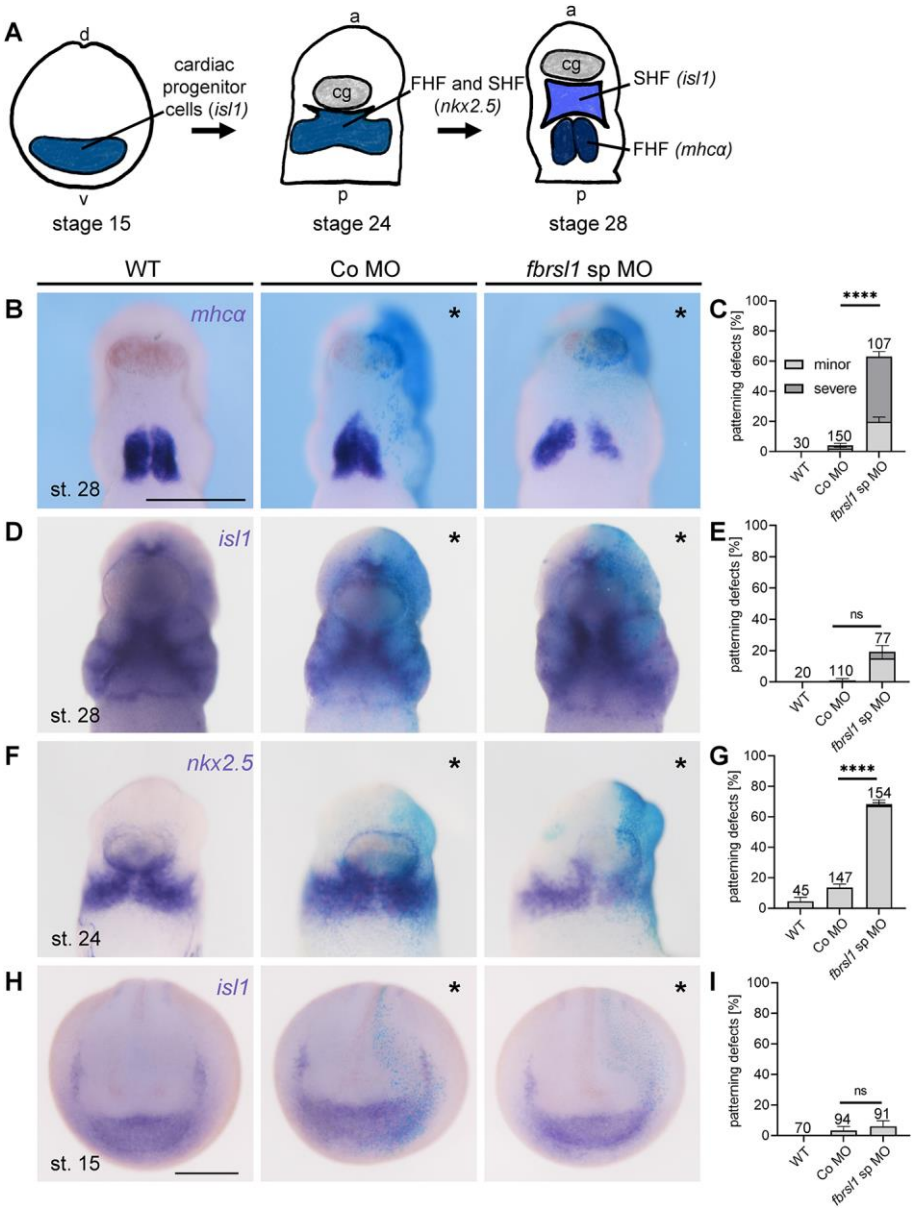

Fig. 3. Fbrsl1 loss-of-function disrupts the development of the first heart field, but not the cardiac progenitor cells. A Schematic illustration of the key steps in *Xenopus* heart development. At stage 15, cardiac progenitor cells are located anterior in a crescent-like structure (marked by *isl1* expression), which gives rise to two separate populations, the first heart field (FHF) and the second heart field (SHF). At stage 24, *nkx2.5* is expressed in both heart fields, while at stage 28 the two cell populations can be distinguished using the markers *mhcα* (FHF) and *isl1* (SHF). **B-I** Embryos were injected at the four-cell stage into one dorsal blastomere with 5 ng - 7.5 ng (B-G) or 7.5 ng - 10 ng (H,I) Co MO or *fbrsl1* sp MO and 80 pg *lacZ* RNA for lineage tracing, cultured to the respective stages and analyzed by in situ

hybridization. *marks the injected side, scale bars = 500 µm. Embryos are shown from the ventral (B-F) or the anterior side (H). **B** Stage 28 embryos analyzed by *mhcα* whole mount in situ hybridization. *fbrsl1* sp MO injected embryos show a reduction of the first heart field on the injected side (minor defect is shown). **C** Graph summarizing the defects in first heart field formation of three independent experiments. **D** Stage 28 embryos analyzed by *isl1* in situ hybridization. Expression is visible in the second heart field. The *fbrsl1* sp MO injected side shows normal expression. **E** Graph summarizing the defects in second heart field formation of three independent experiments (wild-type only 2 experiments). **F** Embryos analyzed by *nkx2.5* whole mount in situ hybridization at stage 24. Expression can be observed in the first and second heart field. The *fbrsl1* sp MO injected side shows reduced expression (minor defect is shown). **G** Graph summarizing the results of three independent experiments shown in F. **H** Whole mount in situ hybridization showing *isl1* expression in the cardiac progenitor cells. The *fbrsl1* sp MO injected side shows normal expression. **I** Graph summarizing the defects of cardiac progenitor cells of three independent experiments. S.e.m. and number of evaluated embryos are indicated in all graphs, ns = not significant, **** $p < 0.0001$ (one-way ANOVA). Abbreviations: (a) anterior, (d) dorsal, (p) posterior, (v) ventral.

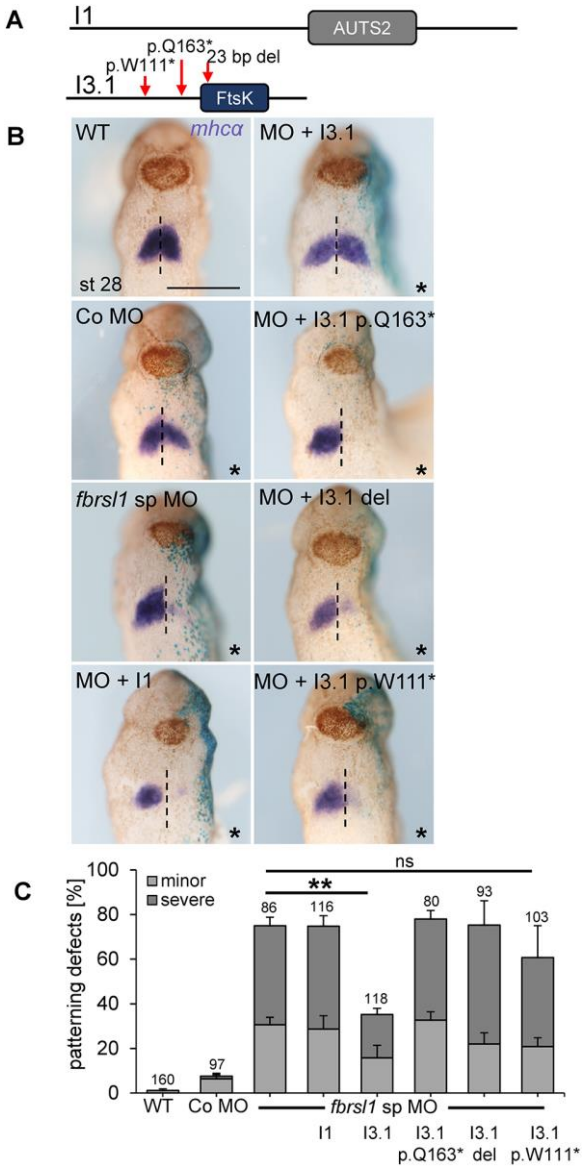

Fig. 4. Defects in *mhcα* patterning are rescued by the human short N-terminal FBRSL1 isoform 3.1. A Scheme of the FBRSL1 isoform 1 and the short N-terminal isoform 3.1. Red arrows indicate the position of the three patient variants. **B** 7.5 ng of the respective morpholino oligonucleotides and 150 pg of the plasmids were injected in one dorsal blastomere at the four-cell stage. 100 pg *lacZ* RNA was co-injected as lineage tracer. Representative embryos at stage 28/29 are shown from the ventral side, injected constructs are indicated. (*) marks the injected side, blue ß-galactosidase staining is visible. Scale bar = 500 µm. **C** The graph summarizes the percentage of *mhcα* patterning defects of three independent experiments. S.e.m. and numbers of analyzed embryos are indicated. ***$p < 0.002$, ns = not significant, $p = 0.06$ (one-way ANOVA).

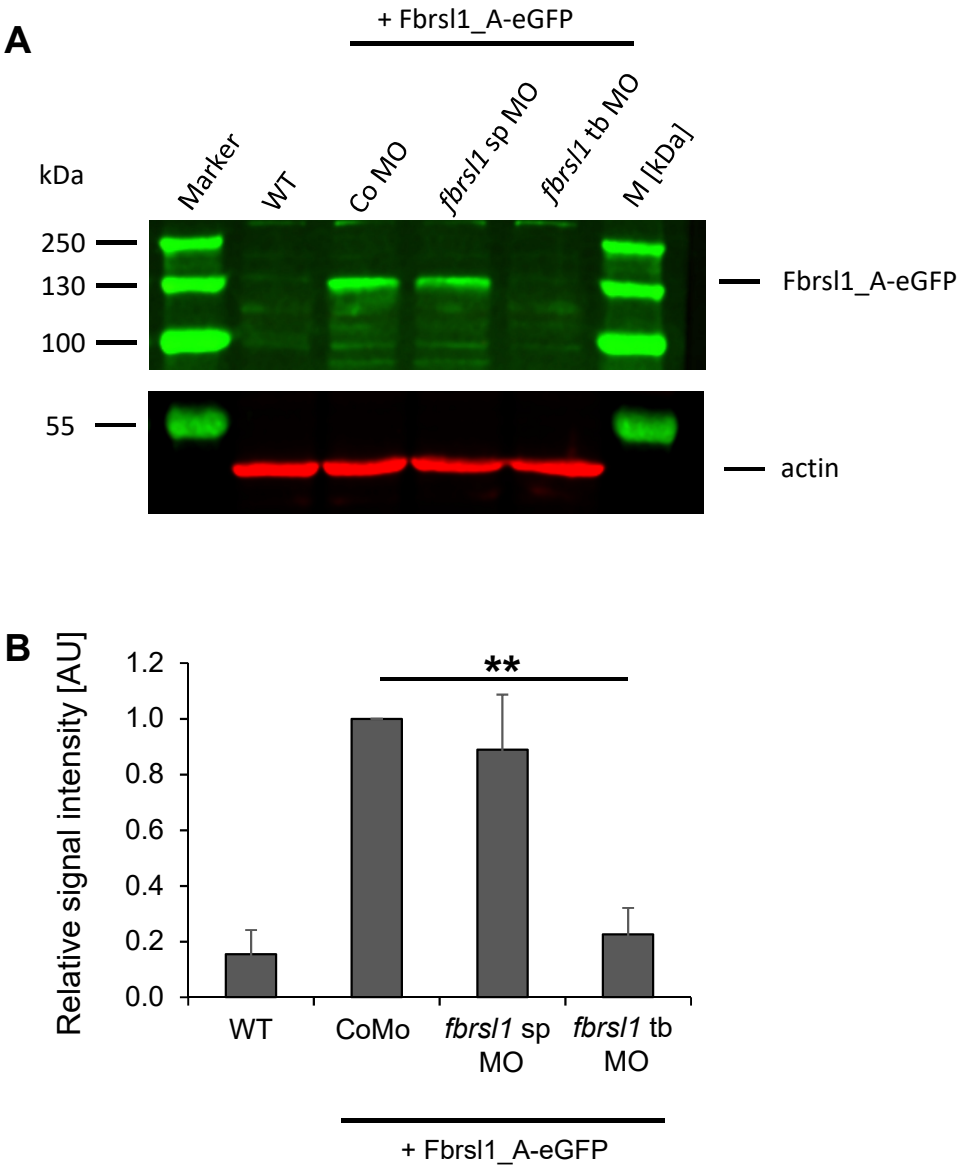

Fig. S1. *fbrsl1* tb MO efficiently inhibits the translation of a *Xenopus* GFP-tagged Fbrsl1 isoform (Fbrsl1_A-eGFP). A One-cell stage embryos were injected with 10 ng Co MO, *fbrsl1* sp MO or *fbrsl1* tb MO together with 100 pg *fbrsl1_A-eGFP* RNA, a shorter Fbrsl1 transcript, isolated from wild-type *Xenopus* embryos. Protein expression was analyzed by western blotting using an α-GFP antibody. In embryos injected with the *fbrsl1_A-eGFP* in combination with Co MO or *fbrsl1* sp MO the protein is detected. However, Fbrsl1_A-eGFP expression is strongly inhibited in embryos co-injected with the *fbrsl1* tb MO. **B** The ratio of signal intensity levels of Fbrsl1_A-eGFP to actin were normalized to the Co MO + Fbrsl1_A-eGFP levels and plotted. The graph shows the mean relative signal intensity (AU, arbitrary units) of Fbrsl1_A-eGFP expression of four independent experiments, s.e.m. are shown, $^{**}p < 0.01$ (one-way ANOVA).

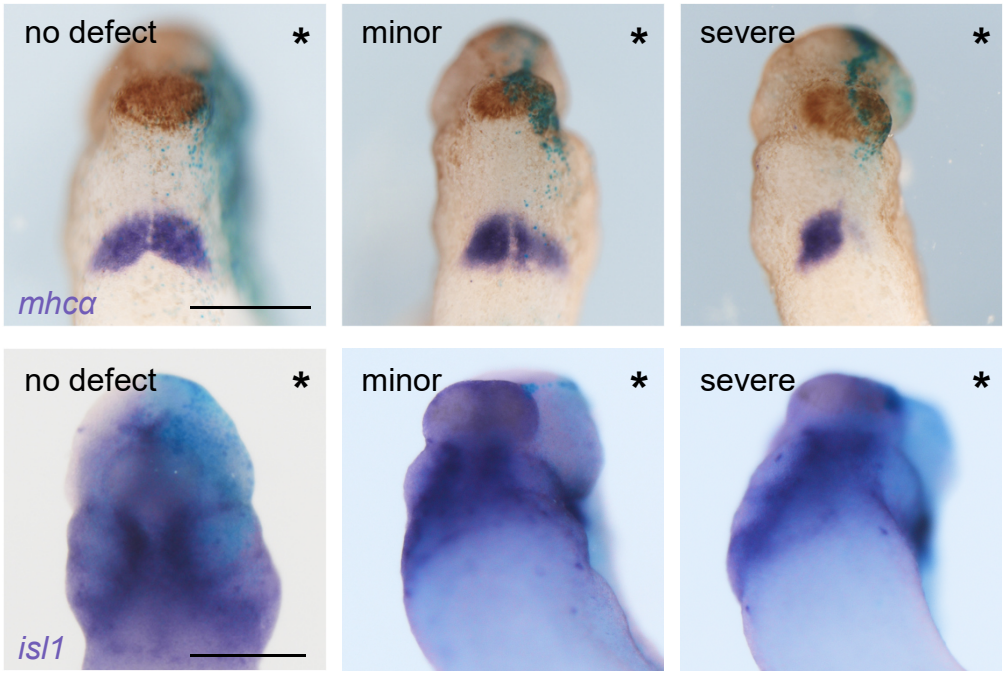

Fig. S2. Categorization of *mhcα* and *isl1* patterning defects

For statistical analyses *mhcα* and *isl1* patterning defects were categorized into minor or severe. Representative embryos for each category are shown. A sterixmarks the injected side.

Fig. S3. *fbrsl1* sp MO and *fbrsl1* tb MO binding sites on *Xenopus laevis fbrsl1.L* and *fbrsl1.S*

A The schematic shows the *fbrsl1* tb MO and *fbrsl1* sp MO binding sites on exon 1 and the exon1/ intron1 boundary. The corresponding morpholino sequences are indicated in the dashed square. **B** shows a section of the *fbrsl1.L* and the *fbrsl1.S* sequences with the corresponding morpholino binding sites marked. Both morpholino oligonucleotides were designed to target the *fbrsl1.L* form. The *fbrsl1* tb MO has 4 mismatches with *fbrsl1.S* and the *fbrsl1* sp MO has 1 mismatch. ATG triplet is shown in bold.

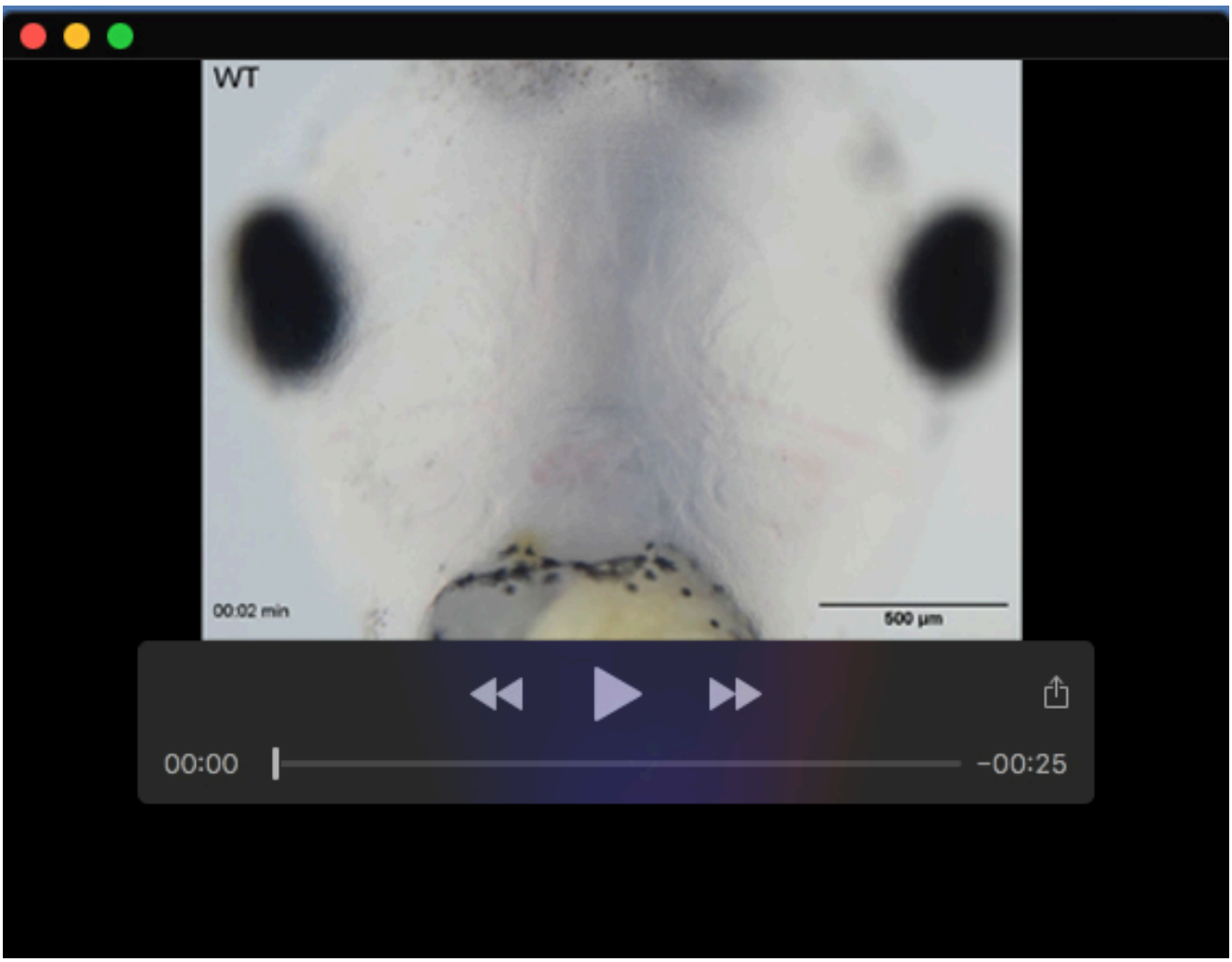

Movie 1. Fbrsl1 loss-of-function leads to malformed hearts in *Xenopus* embryos. Four-cell stage embryos were injected in one dorsal blastomere with 7.5 ng of Co MO, *fbrsl1* sp MO and *fbrsl1* tb MO in combination with 50 pg *mGFP* RNA as lineage tracers. The embryos were anesthetized in 0.1x MBS (modified Barth's saline) containing 0.01% benzocaine. Beating hearts were recorded at stage 44. Embryos are shown from the ventral side. Wild-type.

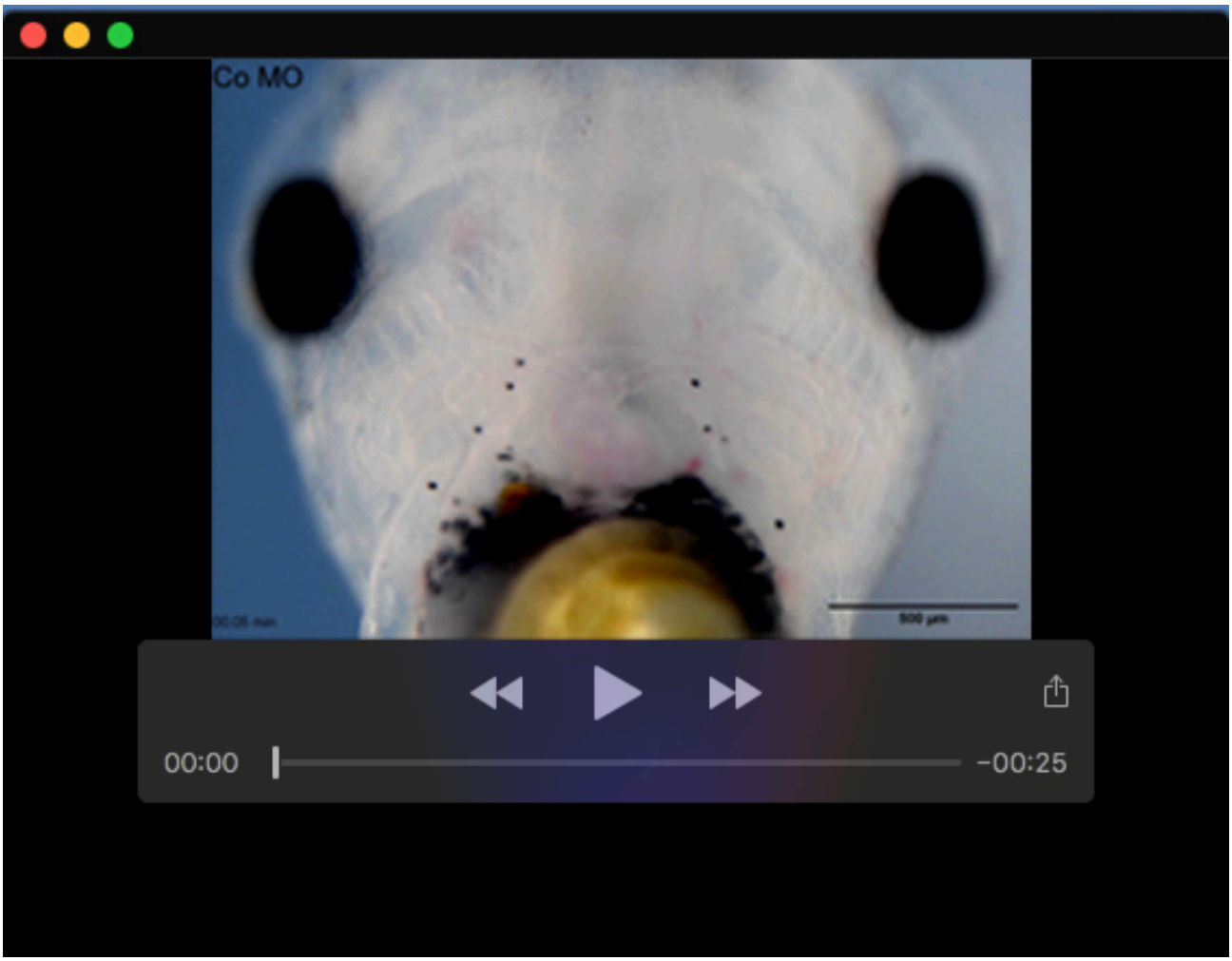

Movie 2. Co MO injected embryos show a dynamic beating of the heart and blood flow through the ventricle and outflow tract. Hearts of *Xenopus* embryos injected with the *fbrsl1* sp MO

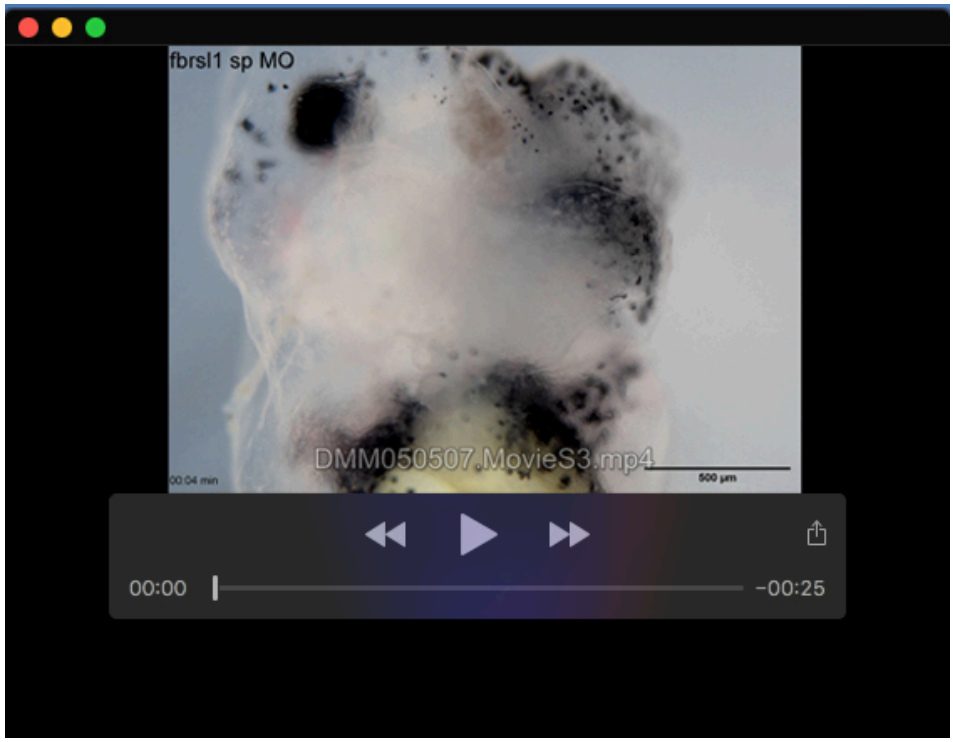

Movie 3. Injected embryos show a dynamic beating of the heart and blood flow through the ventricle and outflow tract. Hearts of *Xenopus* embryos injected with the fbrsl1 sp MO.

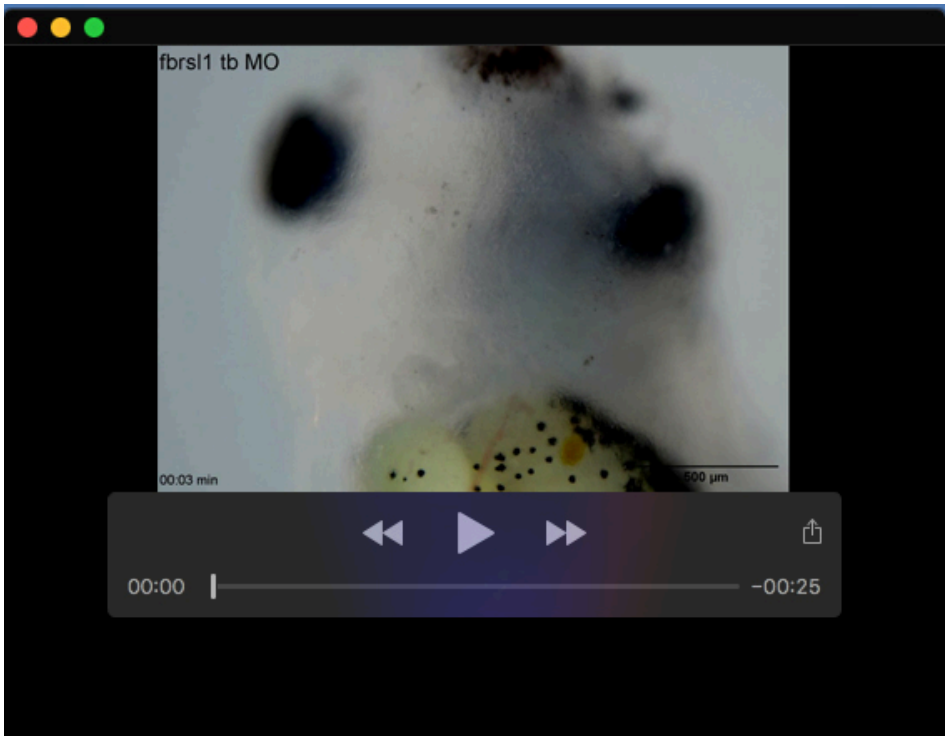

Movie 4. *fbrsl1* tb MO are also able to beat, although they are malformed, have a smaller ventricle and the blood flow is hardly visible.